Proceedings World Geothermal Congress 2023
Beijing, China, April 17 – 21, 2023

Improvement of a Geoejector Design Using an Analytical Model and Data from Theistareykir Geothermal Field, Iceland

Jeffrey Macatangay Andal[1,3], Ragnar Lárusson[1], Ximena Guardia Muguruza[1], Guðrún Sævarsdóttir[1], Yonatan Afework Tesfahunegn[1], Egill Júlíusson[1], Karl E. Sveinsson[2], Vijay Chauhan[1,3], María Sigríður Guðjónsdóttir[1,3]

[1]Department of Engineering, Reykjavik University, Menntavegur 1, 102 Reykjavik, Iceland

[2]Landsvirkjun, Háaleitisbraut 68, 103 Reykjavík, Iceland

[3]GRÓ-GTP, Urdarhvarf 8 (B), 203 Kópavogur, Iceland

jeffrey21@ru.is

Keywords: Geojector, analytical model, low-pressure, high-pressure, Theistareykir

ABSTRACT

To utilize a low-pressure geothermal well, a subsonic ejector system (referred to as subsonic geoejector) was developed and tested at the Theistareykir Geothermal Field in 2020 and 2021. The system connected a low-pressure geothermal well to a nearby high-pressure well to induce flow from the low-pressure well under otherwise unfavorable back pressure. The subsonic geoejector has the same working principle as an industrial ejector used in many industries. However, unlike traditional ejectors, it is faced with challenges involving two-phase geothermal fluids and highly variable inflow conditions. From analysis with an analytical model of the subsonic ejector, it was found that it cannot accelerate the high-pressure fluid enough to create an underpressure that will induce flow from the low-pressure well under real operating conditions. To address this problem, this paper will introduce a supersonic geoejector that was designed and analyzed with an analytical model. The result of the model is promising, and it is found that the new setup could potentially increase the pressure of geothermal fluid from low-pressure well up to 2.4 bar, which would add up to 0.8 MWe for power generation.

1. INTRODUCTION

Drilling geothermal wells is one of the primary cost contributors to any geothermal project, ranging from 32 to 37% of a project's total investment (Gehringer, M. and Loksha, V.C., 2012). In addition to the cost, the drilling also involves high risk with success rates of wells varying from 59 to 83% depending on the project phase (IFC, 2013). One of the reasons a well is deemed unsuccessful is when the pressure in the well is too low to be connected to the steam gathering system. To address this problem at the Theistareykir Geothermal Field, a rudimentary subsonic ejector system, referred to as subsonic geoejector, was fabricated and tested in 2020 and 2021. These tests aimed to connect the high-pressure geothermal well ÞG-11 to induce flow from the low-pressure geothermal well ÞG-15 by creating a localized underpressure where the two streams meet.

An ejector is a static device that converts the pressure of a high-pressure primary stream into kinetic energy to draw or entrain a fluid from a low-pressure secondary source. The two streams will then mix and discharge into a diffuser to convert the kinetic energy back into increased pressure. Ejectors are relatively common and have a variety of applicability in different industries such as refrigeration, power generation, and chemical sectors. Additionally, this technology has a minimal maintenance requirement due to their nonmoving parts, low operating expenses, and no constraints on the working fluid (Besagni, G., 2019).

As to the authors' knowledge, limited information can be found regarding the application of ejectors to recover geothermal fluids from low-pressure wells. In 1999, an ejector apparatus to increase the fluid recovery from geothermal wells was patented (Jung, 1999). However, according to Gutsol, A. F. (2018), the ejector field test did not validate the patent's claim and it was likely caused by the problem on the ejector parameters. Unfortunately, no calculation method for the ejector parameters was disclosed in the patent. In the current work, we refer to the ejector used for this purpose as a geoejector.

To determine the geometrical parameters and analyze the performance of a geoejector, this study considered several studies that investigated the effect of geometrical parameters on supersonic ejector performance. Keenan and Neuman proposed a 1-D constant pressure mixing ejector theory to analyze the performance of an ejector (Keenan, J. H. & Neuman, E. P., 1942). This model was later improved by considering the thermodynamic irreversibility and real gas behavior (Keenan, J. H. & Neuman, E. P., 1950). Another study proposed that after the primary flow is discharged from the ejector's nozzle exit, it fans out without mixing with the entrained flow and induces the latter to a converging duct within the mixing chamber. This converging duct accelerates the entrained flow to a sonic velocity at some point inside the converging duct known as the "effective area" or the hypothetical throat. Downstream of the hypothetical throat the mixing of the two streams occurs with a uniform pressure (Munday, J. T. & Bagster, D. F., 1977). Studies went on further and assumed that the hypothetical throat occurs inside the constant area mixing section of the ejector. Huang et al. built a 1-D model to predict performance while the ejector is in critical mode or double choking (Huang, B. J., Chang, J. M., & Wang, C. P., 1999). One of the challenges of the 1-D model for ejectors was determining the speed of sound in a two-phase flow. To circumvent this problem, the mass flux maximization criterion was introduced by Ameur et. al (Ameur, K., Aidoun, Z., and Ouzzane, M., 2016). Chen et al. developed a theoretical model that analyses ejector performance under critical and sub-critical modes (Chen, W., Shi, C., Zhang, S., Chen, H., Chong, D., & Yan, J., 2017). The model from Chen et al. compared reasonably to the experimental and theoretical results from the literature (Huang, B. J., Chang, J. M., & Wang, C. P., 1999, Aphornratana S, Chungpaibulpatana S, Srikhirin P., 2001).

The field tests at Theistareykir employed a rudimentary subsonic geoejector. The high-pressure geothermal well was operated far below its nominal operating pressure due to the limitation of the separator used during the tests. This resulted in the pressure difference between the wells being significantly lower than it would be under real operations. It was also determined that the subsonic geoejector would not be able to accelerate the high-pressure fluid enough to create a sufficiently low underpressure to induce flow from the low-pressure well. To circumvent this problem, a supersonic geoejector needs to be designed to meet the parameters required in real operations.

In the current work, an analytical model of a supersonic geoejector was made to determine a geoejector design that will maximize the combined power output from the two connected wells from the tests at Theistareykir under realistic operating conditions. The analytical model is largely based on the models developed Huang et al. (Huang, B. J., Chang, J. M., & Wang, C. P., 1999) and Chen et al. (Chen, W., Shi, C., Zhang, S., Chen, H., Chong, D., & Yan, J., 2017). This work is considered a first step in developing a practical and economical geoejector that employs the flow of a high-pressure well to induce flow from a well at lower pressure, thus connecting it to the steam gathering system. The model does not yet address major challenges expected under real operations, such as scaling, two-phase flow, and highly transient inflow.

2. SUPERSONIC GEOEJECTOR

A schematic of the supersonic geoejector is shown in Figure 1. It has the same main components as a typical supersonic ejector used in various industrial applications.

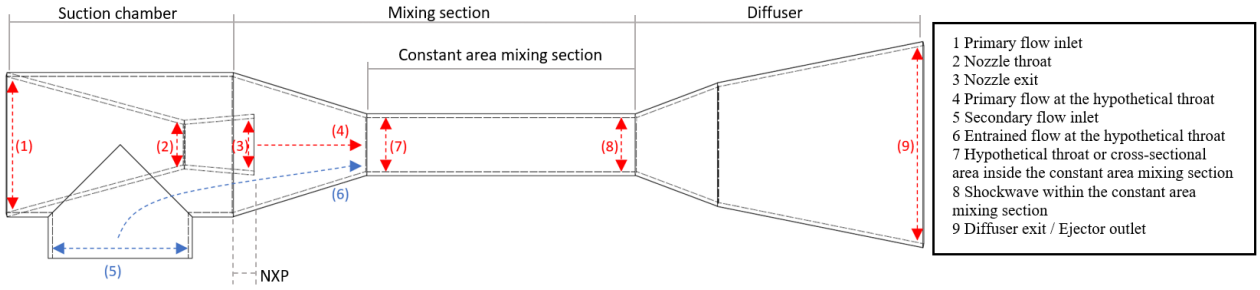

Figure 1: Supersonic geoejector.

The primary fluid is accelerated to supersonic speed through the primary nozzle (steps 1 to 3), thereby creating underpressure in the mixing section that induces flow from the secondary inlet (5). Ideally, the induced or entrained flow accelerates and reaches sonic speed at the hypothetical throat (6), effectively choking the secondary flow. The primary flow leaving the nozzle is assumed to spread without mixing with the entrained flow (4). The two streams start to mix at the hypothetical throat (7) at constant pressure. The flow remains supersonic within the section until it is compressed and decelerated through a shockwave (8). In reality, a train of shockwaves is formed, but analytical models typically simplify the process and consider one normal shockwave. The flow is then further decelerated in a diffuser (9) to reach a desired back pressure. An example of pressure-enthalpy (Ph) diagram of these processes, and pressure and Mach number profile are shown in Figure 2 and Figure 3, respectively.

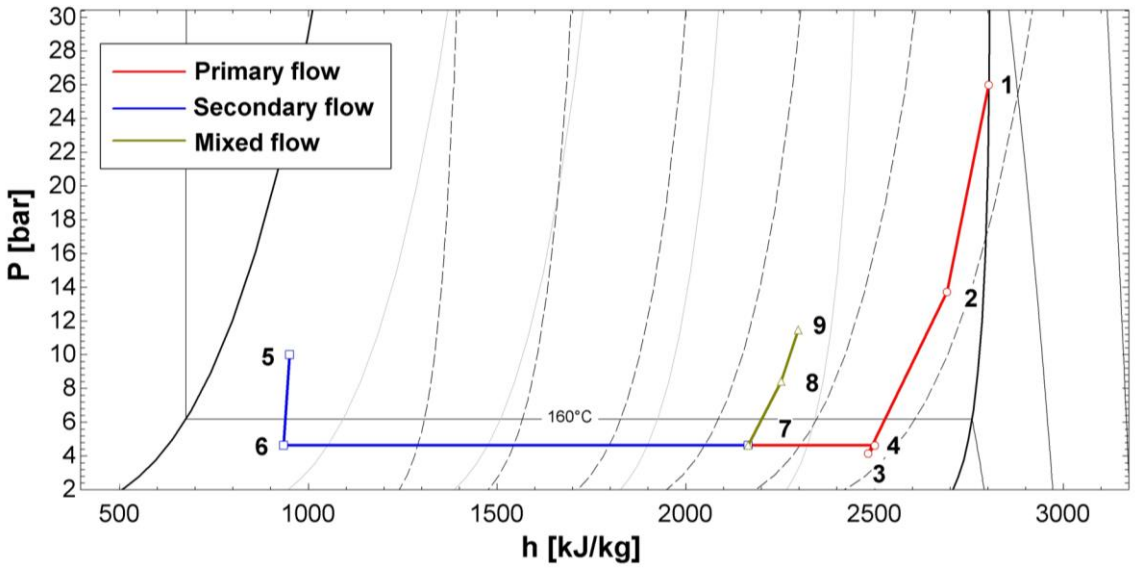

Figure 2: Ph diagram of the supersonic geoejector flow processes.

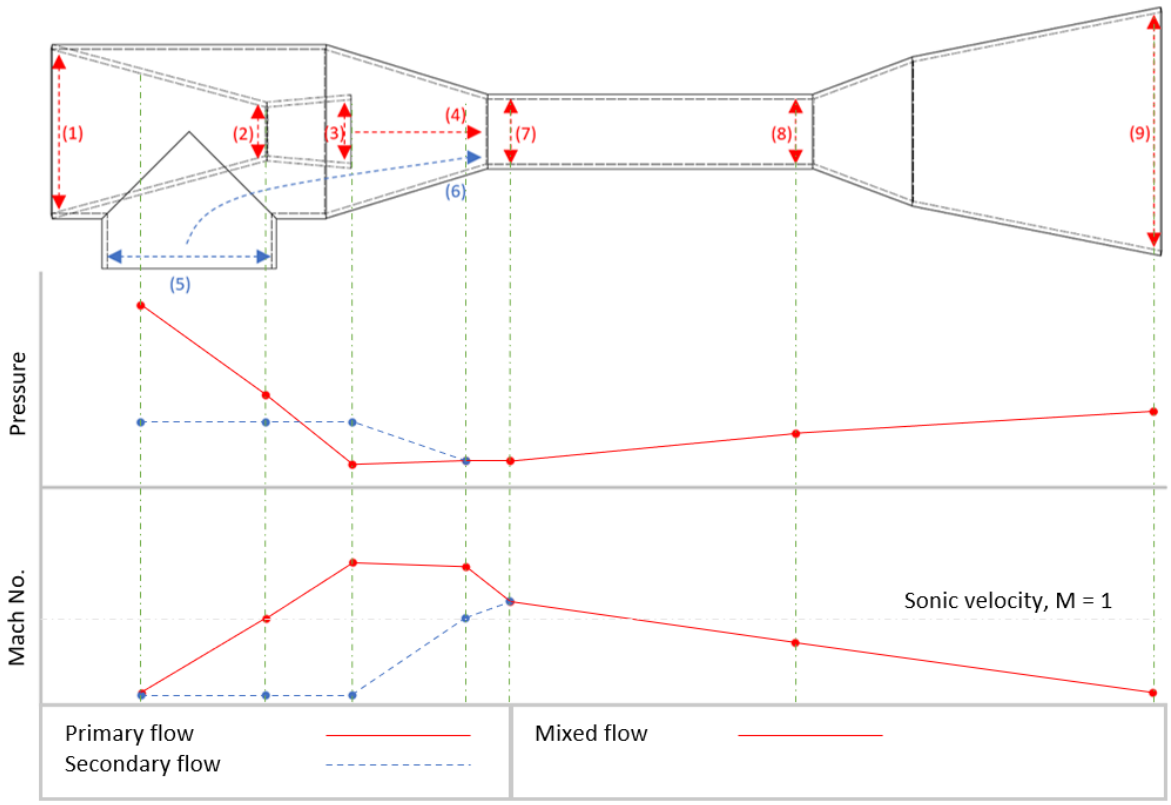

Figure 3: Typical Pressure and Mach No. profiles through the geoejector.

3. ANALYTICAL MODEL FOR DESIGNING A SUPERSONIC GEOEJECTOR

3.1 Operating Conditions

The proposed geoejector design is intended to connect wells ÞG-11 and ÞG-15 in Theistareykir as the high-pressure fluid source (primary) and the low-pressure source (secondary), respectively.

Well ÞG-11 is a production well that was drilled in July 2016 and is in Theistareykir Geothermal Production Field. Well ÞG-15 is located on the same pad and was drilled in March 2017 (Mkangala, A., 2017, Egilson, T., 2019). Further information about the wells is shown in Table 1.

Table 1: Properties of wells ÞG-11 and ÞG-15 (Egilson, T., 2019).

Well name	Depth (m)	Measured mass flow rate at reported wellhead pressure(kg/s)	Reported well head pressure (bar-g)	Enthalpy (kJ/kg)	Well head potential (MWe)[1]	Status[1]
ÞG-11	2224	26	30	2700	14.4	In use
ÞG-15	2260	14	8.7	950	2.0	Not in use

[1] (Knútsson, V., Geirsson, S. B., Hjartarson, H., & Emilsson, J. A., 2018).

The wellhead pressure of ÞG-11 is currently reduced to the steam gathering system pressure (9.5 – 10 bar-g) through orifice plates. On the other hand, the wellhead pressure of ÞG-15 is not high enough to reliably enter the system (i.e. minor fluctuations in the line pressure cause the well to choke) and has therefore not been in use.

From the recent well measurement data and recommendations from the power plant operators, the pressure from ÞG-11 considered in this paper ranges from 10 to 25 bar-g. Additionally, the well was determined to have a maximum mass flow rate of 30 kg/s. Well ÞG-15 has a maximum wellhead pressure of 9 bar-g. However, there is no recent well measurement to determine its maximum mass flow rate.

3.2 Analytical Model of the Supersonic Geoejector

The assumptions used in the analytical model are based on the information gathered from the first geoejector field tests and other available literature, primarily Chen et al. and Huang et al. (Chen, W., Shi, C., Zhang, S., Chen, H., Chong, D., & Yan, J., 2017, Huang, B. J., Chang, J. M., Wang, C. P., & Petrenko, V. A., 1999):

1. The flow from both primary and secondary sources is assumed to follow the ideal gas law.
2. The following values have previously given acceptable results in the prediction of outlet pressure of the subsonic geoejector tested in 2020 and 2021 and will be adapted for the supersonic geoejector:

   a. constant ratio of specific heat (C_p/C_v), $k = 1.327$;
   b. coefficient of frictional and mixing losses, $c_l = 0.84$; and
   c. isentropic efficiencies of the nozzle and entrained flow, $\eta_n = 0.90$.
3. The primary flow leaving the nozzle and the entrained secondary flow will not start to mix until they reach the hypothetical throat (location 7 in Figure 1).
4. At the hypothetical throat, the two streams start to mix with uniform pressure equal to the pressure at the secondary flow at the hypothetical throat.
5. The entrained flow is choked at the hypothetical throat.
6. The inner walls of the supersonic geoejector are adiabatic.

To ensure that the analytical model would fit the current case, the following assumptions and constraints were added in the model:

1. The exit pressure of the supersonic geoejector should not fall under 9.5 bar-g to avoid problems from surges in the steam gathering pipeline.
2. The maximum pressures at the primary and secondary inlet considered in the model are 25 bar-g and 9 bar-g, respectively.
3. The model treats the two-phase flow from well ÞG-15 as a homogenous mixture, i.e., it uses weighted density and enthalpy, and common pressure and temperature. This is a significant simplification given the low quality of the steam, which raises the importance of phase separation and uncertainty regarding the flow regime. However, at this stage, it is a necessary simplification to get an initial geoejector design.
4. While there is no recent available data to determine the maximum mass flow from ÞG-15, the mass flow is considered similar to the values in Table 1.
5. To ensure that the fluid from the secondary source will be effectively entrained, the pressure of the primary flow at the nozzle exit should be less than or equal to the pressure of the secondary flow at the hypothetical throat.
6. To avoid a shockwave due to sudden change in flow direction, the area of the nozzle exit should be less than the area of the constant area mixing section.
7. The mixture in the constant area mixing section is homogeneous.
8. Effects of liquid-vapour phase-change are not accounted for in the model.

Following the setup described in Section 2 and the assumptions and constraints described in this section, the geometric parameters for the supersonic geoejector can be calculated by adapting the formulas from Chen et al. (Chen, W., Shi, C., Zhang, S., Chen, H., Chong, D., & Yan, J., 2017). Further, the thermophysical properties of the fluid were obtained using CoolProp (Bell, I. H., Wronski, J., Quoilin, S., & Lemort, V., 2014) wherein the equation of state of ordinary water/steam was largely based on IAPWS 95 formulation (Wagner, W., & Pruss, A, 2002).

Nozzle throat (2): to get a supersonic flow from the nozzle, the throat should accelerate the primary fluid until it reaches sonic flow. With this, the pressure, p_2, and the enthalpy, h_2, at the throat, can be determined by iterating p_2 until the fluid velocity, v_2^*, becomes critical, i.e. equal to sonic velocity, a_2^*, as shown in Equation 1 and 2, respectively (subscript numbers refer to locations in Figure 1).

$$v_{2|p2}^* = \sqrt{2\left(h_1 - h_{2|p_2}^*\right) + {v_1}^2} \tag{1}$$

$$a_{2|p2}^* = \sqrt{\frac{kp_2}{\rho_{2|p_2}^*}} \tag{2}$$

Considering the isentropic efficiency, η_n, of the compressible flow in the nozzle, the enthalpy obtained from the isentropic enthalpy, h_2^*, can be adjusted using Equation 3.

$$h_2 = h_1 - \eta_n(h_1 - h_2^*) \tag{3}$$

With the calculated pressure, p_2, obtained from Equations 1 and 2, and adjusted enthalpy, h_2, from Equation 3, the velocity and density at the throat can then be determined. These values, along with the mass flow rate, $\dot{m}_1$, are needed to get the area at the throat, A_2, as shown in Equation 4.

$$A_2 = \frac{\dot{m}_1}{v_2\rho_2} \tag{4}$$

Nozzle exit (3): in this section of the model, it is important to assign a temporary value for the diameter of the nozzle exit, D_3. This can later be optimized to make sure that all the constraints are met. After assigning a value, the pressure at the nozzle exit, p_3, will be iterated until the two formulas for velocity, as shown in Equations 5 and 6, give equal results.

$$v_3 = \frac{\dot{m}_1}{\rho_{3|p_3}A_3} \tag{5}$$

$$v_3' = \sqrt{2\left(h_2 - h_{3|p_3}\right) + {v_2}^2} \tag{6}$$

Entrained flow at the hypothetical throat (6): the entrained secondary flow is assumed to reach sonic, or choking condition, at the hypothetical throat. To calculate the pressure, p_6, and enthalpy, h_6, of the secondary flow in this area, the value of the pressure should be iterated until the fluid velocity, v_6^*, becomes critical, i.e. equal to sonic velocity, a_6^*, as shown in Equation 7 and 8, respectively.

$$v_{6|p6}^* = \sqrt{2\left(h_5 - h_{6|p_6}^*\right) + {v_5}^2} \tag{7}$$

$$a^*_{6|p_6} = \sqrt{\frac{kp_6}{\rho^*_{6|p_6}}} \tag{8}$$

Considering the isentropic efficiency, η_n, the enthalpy obtained from the isentropic enthalpy, h^*_6 can be adjusted using Equation 9.

$$h_6 = h_5 - \eta_n(h_5 - h^*_6) \tag{9}$$

With the calculated pressure, p_6, from Equation 7 and 8, and adjusted enthalpy, h_6, from Equation 9, the velocity and density of the secondary flow before the hypothetical throat can then be calculated. These values, along with the mass flow rate, $\dot{m}_5$, are needed to get the area of the hypothetical throat occupied by the entrained flow, A_6, as shown in Equation 10.

$$A_6 = \frac{\dot{m}_5}{v_6\rho_6} \tag{10}$$

Primary flow at the hypothetical throat (4): it was assumed that the two streams start to mix with uniform pressure equal to the pressure of the entrained flow at the hypothetical throat, p_6. Additionally, it was assumed that the flow from the nozzle exit to the hypothetical throat is isentropic. In contrast, a loss coefficient, c_l, is included in calculating the area of the hypothetical throat occupied by the primary flow, A_4, as shown in Equation 11.

$$A_4 = \frac{c_l\dot{m}_1}{v_4\rho_4} \tag{11}$$

Hypothetical throat or cross-sectional area inside the constant area mixing section (7): the sum of the areas of the primary and entrained flow before the hypothetical throat will then be equal to the area of the constant area mixing section, as shown in Equation 12.

$$A_7 = A_6 + A_4 \tag{12}$$

It was further assumed that the two streams will start to mix inside the constant area mixing section. A momentum balance relationship with the inclusion of losses can be used to determine the velocity, v_7, as shown in Equation 13.

$$v_7 = \frac{c_l(\dot{m}_1 v_4 + \dot{m}_5 v_6)}{\dot{m}_1 + \dot{m}_5} \tag{13}$$

Additionally, the enthalpy, h_7, can be determined using the energy balance relation as shown in Equation 14.

$$h_7 = \frac{\dot{m}_1\left(h_4 + \frac{{v_4}^2}{2}\right) + \dot{m}_5\left(h_6 + \frac{{v_6}^2}{2}\right)}{\dot{m}_1 + \dot{m}_5} - \frac{{v_7}^2}{2} \tag{14}$$

Shock wave within the constant area mixing section (8): The flow is compressed and decelerated to subsonic velocities through a shockwave. To determine the flow property changes in this section, the density, ρ_8, will be iterated until it satisfies the conditions for the continuity, momentum, and energy equation, as shown in Equations 15-17. The pressure and enthalpy obtained will then be used to determine the remaining properties in this section, see Equation 18. The iteration will continue until $\rho_8 = \rho'_8$.

$$v_{8|\rho_8} = \frac{v_7\rho_7}{\rho_8} \tag{15}$$

$$p_{8|\rho_8} = p_7 + {v_7}^2\rho_7 - {v_{8|\rho_8}}^2\rho_8 \tag{16}$$

$$h_{8|\rho_8} = h_7 + \frac{{v_7}^2}{2} - \frac{{v_{8|\rho_8}}^2}{2} \tag{17}$$

$$\rho'_{8|\rho_8},\ s_{8|\rho_8},\ T_{8|\rho_8} = f\left(p_{8|\rho_8}, h_{8|\rho_8}\right) \tag{18}$$

Diffuser exit or Geoejector exit (9): the diffuser will further decelerate the fluid and increase the pressure. To obtain the properties at the diffuser exit, the steady one-dimensional incompressible continuity equation, as shown in Equation 19, is used to calculate the velocity, v_9, after the diffuser.

$$v_9 = v_8\left(\frac{A_8}{A_9}\right) \tag{19}$$

After obtaining the velocity, the enthalpy, h_9, at the diffuser exit could be obtained through the energy balance equation, as shown in Equation 20. While the rest of the properties at the diffuser exit could be obtained by assuming that the entropy after the shock, s_8, is equal to the entropy at the diffuser exit, s_9.

$$h_9 = h_8 + \frac{{v_8}^2}{2} - \frac{{v_9}^2}{2} \tag{20}$$

The model's flowchart showing the processes in the calculation for the geometrical parameters of the supersonic geoejector is shown in Figure 4.

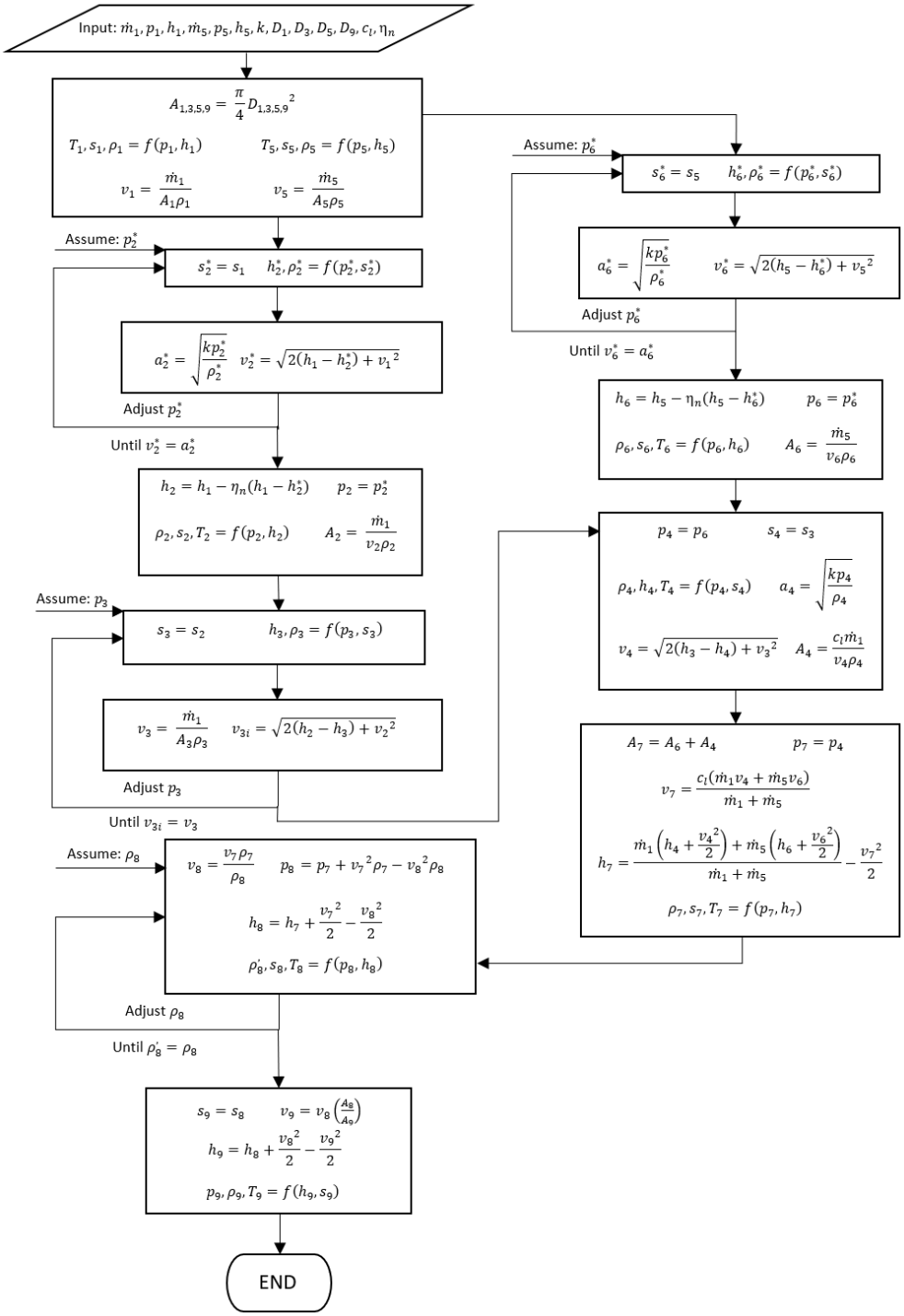

Figure 4: Analytical model of supersonic geoejector.

3.3 Primary Nozzle Position and Constant Area Mixing Section Length

Primary nozzle position (NXP) is the distance between the nozzle exit and the entrance of the mixing section or the converging section going to the hypothetical throat (See Figure 1). This geometrical parameter is important as it directly impacts the entrainment ratio, *ER*, or the ratio between mass flow rate from secondary and primary flow, as shown in Equation 21. NXP will be calculated using the formula presented by Ding et al. (Ding, Z., Wang, L., Zhao, H., Zhang, H., and Wang, C., 2016), as shown in Equation 22.

$$ER = \frac{\dot{m}_5}{\dot{m}_1} \tag{21}$$

$$NXP = \left(\sqrt{0.083 + 0.76\, ER} - 0.29\right) \frac{D_3}{2^{\alpha}} \tag{22}$$

Where α is an empirical constant that is typically between 0.07 and 0.09. Here, a value of 0.07 is used.

Length of the constant area mixing section (L_{CAMS}): Studies in the literature have made various conclusions regarding the impact of the length of the constant area mixing section on the entrainment ratio. However, studies showed that as it increases, the mixing effect

between the primary and induced flows improves. This efficient mixing decreases the speed differential between the two flows. As a result, the mixed stream becomes more uniform, and the ejector may work at a higher back pressure and gain a higher-pressure ratio. The achievable back pressure, however, declines when the ratio of the constant area mixing section length, L_{CAMS}, to its diameter, D_7, exceeds 5 (Chen, W., Chong, D., Yan, J., and Liu, J., 2013). With this, a ratio of 5 is used in the current work (see Equation 23).

$$\frac{L_{CAMS}}{D_7} = 5 \tag{23}$$

These geometrical parameters are based on empirical observations and parameters obtained from the analytical model presented in the previous subsection. Optimizing these geometrical parameters requires Computational Fluid Dynamics and experimental validation, which is not covered in this paper.

4. RESULTS AND DISCUSSION

In consideration of the constraints described in Section 3.2, the geometrical parameters of the supersonic geoejector obtained from the analytical model were used to determine the working parameters in terms of inlet pressures and the resulting outlet pressure, as shown in Figure 5.

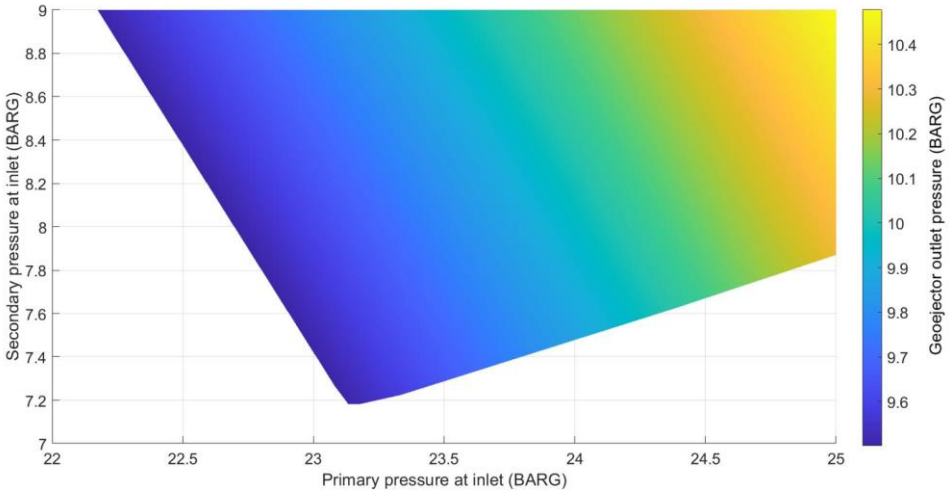

Figure 5: Geoejector exit pressure for varying input pressures.

Figure 5 shows that the induced pressure, i.e. the difference between the secondary flow inlet pressure and the geoejector's outlet pressure, ranges from 0.5 to 2.4 bar. As the pressure from the primary flow varies, there is a corresponding minimum pressure that the secondary flow should meet to ensure that the output of the geoejector is not susceptible to surges in the steam gathering system. This sets the operational range of the geoejector. The induced secondary flow is the result of transfer of energy from the primary flow to the secondary flow. When the pressure from the primary flow is lower than 23.1 bar-g, there is a need to increase the pressure from the secondary flow. This is needed because as the pressure at the primary flow inlet decreases, the primary mass flow rate decreases, which reduces the available energy from the primary flow that can be transferred to the secondary. Furthermore, if the primary inlet pressure falls below 22.2 bar-g, the energy from the primary flow will not be enough to induce flow from the secondary inlet while reaching the desired minimum outlet pressure. Changes in the geometric parameters of the geoejector are required to handle lower than 22.2 bar-g inlet pressure of the primary flow. However, this would limit the mass flow from well ÞG-11 and decrease its power output. On the other hand, when the pressure from the primary flow is greater than 23.1 bar-g, there is still a need to increase the pressure from the secondary flow. This increase is necessary to be certain that the pressure of the secondary flow in the hypothetical throat remains higher than the pressure of the primary flow leaving the nozzle. This scenario can be observed in Figure 6.

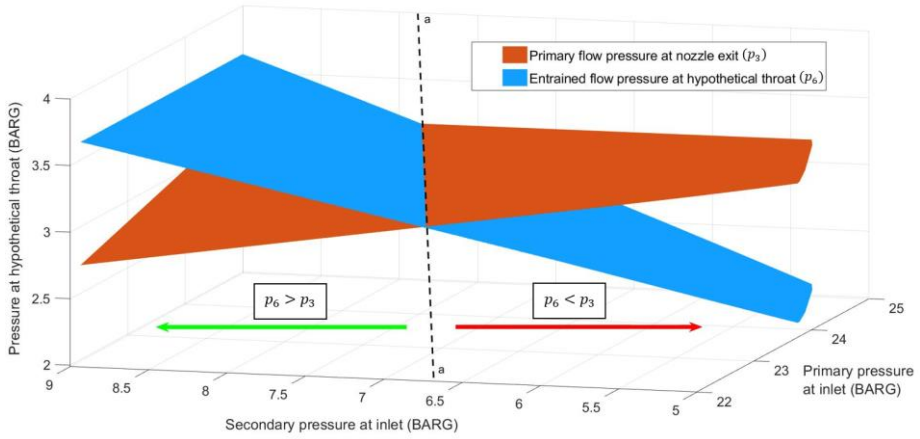

Figure 6: Pressure of primary flow at nozzle exit and entrained flow at the hypothetical throat.

Figure 6 shows that the area to the right of line a-a is where the primary flow pressure at the nozzle exit is greater than the pressure from the entrained flow at the hypothetical throat. If the geoejector operates at this condition the entrainment ratio is expected to decrease due to unfavorable pressure difference. This area could be reduced by increasing the diameter of the nozzle exit to decrease the primary flow pressure even further. However, as mentioned in the constraints in Section 3.2, the area of the nozzle exit should not be greater than the area of the constant area mixing section.

The relationship between the induced pressure of the secondary flow and entrainment ratio is shown in the upper portion of Figure 7. When induced pressure is at its lowest, 0.5 bar, the entrainment ratio is at maximum, 50.4%. On the other hand, if the induced pressure is at maximum, 2.4 bar, the entrainment ratio will be at lowest, 25.8%. This range of entrainment ratio and induced pressure is optimal as the values obtained for the mass flow for both wells are near their maximum, see the lower graph of Figure 7. Note that the areas plotted in Figure 7 are determined by the working parameters shown in Figure 5.

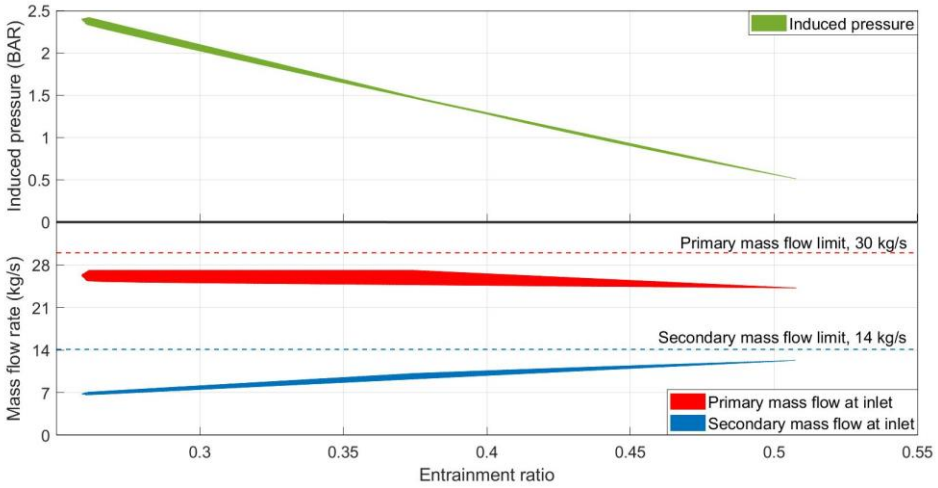

Figure 7: Induced pressure and mass flow vs entrainment ratio.

Since the supersonic geoejector was designed to be connected to the geothermal power plant, the estimated power generation with the supersonic geoejector under the working parameters was compared to the generated power from only using well ÞG-11 (without geoejector), as shown in Figure 8. Note that the geoejector performance is only compared to well ÞG-11 because well ÞG-15 has an outflow pressure lower than the operating pressure, making it unusable for power generation. Additionally, the pressure at the primary inlet of the geoejector was based on the expected steam line pressure at the location where the geoejector will be installed.

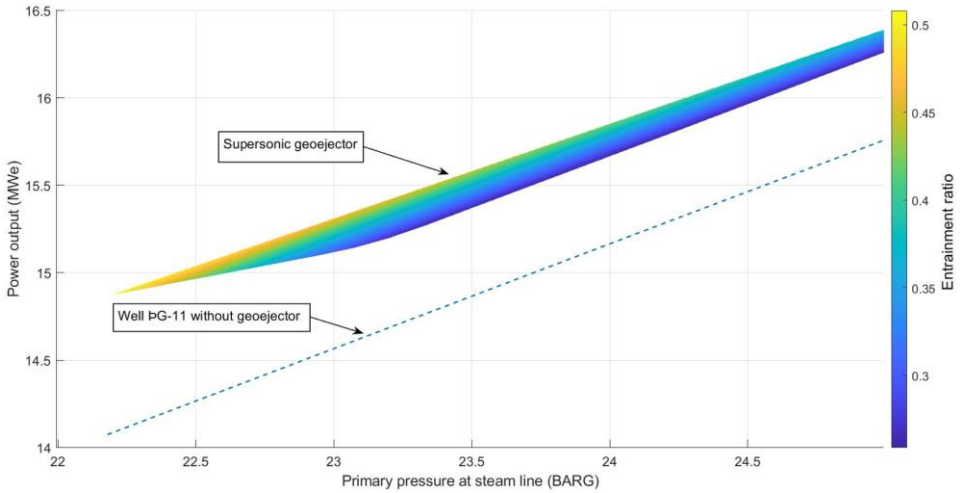

Figure 8: Power output potential from using supersonic geoejector vs. from well ÞG-11 only (without geoejector).

The result of the model suggests that the added power generation from the supersonic geoejector could vary from 0.5 to 0.8 MWe or 25% to 40% of the wellhead potential of ÞG-15. The figure further shows that the highest added power output from ÞG-15 is only achievable when the output from ÞG-11 is limited, however, the total power output declines as the input from ÞG-11 is reduced (entrainment ratio increases). Note that the variation in the power output of the supersonic geoejector is dependent on the inlet pressures of both primary and secondary flow.

5. CONCLUSION

The improved design of the supersonic geoejector aims to address the limitation of the subsonic geoejector tested in 2020 and 2021, i.e. to handle more realistic operating conditions which demand higher difference in pressure of the connected wells.

The analytical model provided the operational range of the supersonic geoejector. It also showed the relationship between the induced pressure and entrainment ratio, wherein the induced pressure will vary from 0.5 to 2.4 bar with a corresponding entrainment ratio from 50.4 to 25.8%, respectively. This range of entrainment ratio is optimal considering the constraints of the maximum mass flow from the wells. Further, with the help of the supersonic geoejector, 0.5 to 0.8 MWe or 25% to 40% of the wellhead potential of well ÞG-15 could potentially be utilized.

Lastly, it is important to note that some geometrical parameters have a significant impact on the output of the supersonic geoejector. To improve these geometrical parameters, further studies on the geoejector using Computational Fluid Dynamics and experiments are needed. These studies and experiments should address challenges expected under real operations, primarily concerning two-phase flow and highly transient inflow. Furthermore, future studies modifying the geoejector into multi-stage geoejector could expand the use of this system into different geothermal fields.

ACKNOWLEDGEMENTS

I, Jeffrey Andal, would like to express my sincerest gratitude to GRÓ-Geothermal Training Programme and its staff, Gudni Axelsson, Ingimar Haraldsson, Málfríður Ómarsdóttir, and Vigdís Harðardóttir, for providing me the necessary support to undertake MSc degree in Sustainable Energy Engineering at Reykjavik University.

REFERENCES

Ameur, K., Aidoun, Z., and Ouzzane, M.: Modeling and numerical approach for the design and operation of two-phase ejectors. *Applied Thermal Engineering*, **109**, (2016), 809–818. https://doi.org/10.1016/j.applthermaleng.2014.11.022

Aphornratana S, Chungpaibulpatana S, Srikhirin P. Experimental investigation of an ejector refrigerator: effect of mixing chamber geometry on system performance. Int J Energy Res, **25**, (2001), 397–411.

Besagni, G.: Ejectors on the cutting edge: The past, the present and the perspective. *Energy*, **170**, (2019), 998–1003. https://doi.org/10.1016/j.energy.2018.12.214

Bell, I. H., Wronski, J., Quoilin, S., & Lemort, V. Pure and Pseudo-pure Fluid Thermophysical Property Evaluation and the Open-Source Thermophysical Property Library CoolProp. Industrial & Engineering Chemistry Research, **53(6)**, (2014), 2498–2508. https://doi.org/10.1021/ie4033999

Chen, W., Chong, D., Yan, J., and Liu, J.: The numerical analysis of the effect of geometrical factors on natural gas ejector performance. *Applied Thermal Engineering*, **59(1–2)**, (2013), 21–29. https://doi.org/10.1016/j.applthermaleng.2013.04.036

Chen, W., Shi, C., Zhang, S., Chen, H., Chong, D., and Yan, J.: Theoretical analysis of ejector refrigeration system performance under overall modes. *Applied Energy*, **185**, (2017), 2074–2084. https://doi.org/10.1016/j.apenergy.2016.01.103

Ding, Z., Wang, L., Zhao, H., Zhang, H., and Wang, C.: Numerical study and design of a two-stage ejector for subzero refrigeration. *Applied Thermal Engineering*, **108**, (2016), 436–448. https://doi.org/10.1016/j.applthermaleng.2016.07.104

Egilson, T.: Þeistareykir Eftirlitsmælingar árið 2018, Iceland GeoSurvey report ISOR-2019/029, (2019), 41 pp.

Gehringer, M. and Loksha, V.C.: Geothermal Handbook: Planning and Financing Power Generation. Washington DC: World Bank Group, Energy Sector, (2012).

Gutsol, A. F.: Ejector for Geothermal Well Lifetime Increase, GRC Transaction, **Vol. 42**, (2018), 6.

Huang, B. J., Chang, J. M., Wang, C. P., and Petrenko, V. A: A 1-D analysis of ejector performance. *International Journal of Refrigeration*, **22(5)**, (1999), 354–364. https://doi.org/10.1016/S0140-7007(99)00004-3

IFC: Success of geothermal wells: a global study. International Finance Corporation, World Bank Group, Washington, DC, (2013), 76 pp.

Jung, D. B.: Eductor/ejector apparatus and the process for increasing fluid recovery from geothermal wells. US Patent 5899273A (1999).

Keenan, J. H. and Neumann, E. P.: A simple air ejector. *Journal of Applied Mechanics*, Trans. **ASME 64**, (1942), 75-81.

Keenan, J. H. and Neumann, E. P., and Lustwerk, F.: An investigation of ejector design by analysis and experiment. *Journal of Applied Mechanics*, Trans. **ASME 17**, (1950), 299-309.

Knútsson, V., Geirsson, S. B., Hjartarson, H., and Emilsson, J. A.: Theistareykir Geothermal Power Plant, A Sustainable Construction. GRC Transaction, **Vol. 42**, (2018).

Mkangala, A.: Borehole Geology of Well THG-15 at Theistareykir Geothermal Field, NE-Iceland. Report 18 in: *Geothermal Training in Iceland*, UNU-GTP in Iceland, (2017), 297-316.

Munday, J. T. and Bagster, D. F.: A new ejector theory applied to steam jet refrigeration. *Ind. Eng. Chem. Process. Des. Dev.* **16 (4)**, (1977), 442-449.

Wagner, W., & Pruss, A. The IAPWS Formulation 1995 for the Thermodynamic Properties of Ordinary Water Substance for General and Scientific Use. Journal of Physical and Chemical Reference Data, **31(2)**, (2002), 387–535. https://doi.org/10.1063/1.1461829

NOMENCLATURE

a = Sonic velocity, m/s

α = empirical constant

A = Area, m^2

c_l = Coefficient of frictional and mixing losses

C_p = Specific Heat in constant pressure

C_v = Specific Heat in constant pressure

D = Diameter, cm

ER = Entrainment ratio

h = Enthalpy, kJ/kg

k = Ratio of specific heats (C_p/C_v)

L = Length, cm

$\dot{m}$ = Mass flowrate, kg/s

M = Mach number

NXP = Primary nozzle position, cm

p = Pressure, Bar-g

s = Entropy, kJ/kg-K

T = Temperature, K

v = Fluid velocity, m/s

α = experimental constant

η_n = Isentropic efficiency

ρ = Density, kg/m^3

Subscripts/superscripts

CAMS = Constant area mixing section

1 = Entrance primary flow

2 = Nozzle throat

3 = Nozzle exit

4 = Primary flow at hypothetical throat

5 = Entrance Secondary flow

6 = Secondary flow at hypothetical throat

7 = Constant area mixing section

8 = Area across the shock

9 = Diffuser exit / Geoejector exit

* = Critical values at sonic point